Synthetic Metals 250 (2019) 115–120

Contents lists available at ScienceDirect

Synthetic Metals

journal homepage: www.elsevier.com/locate/synmet

Excited state dynamics of organic semiconductors measured with shot-to-shot correction of scatter and photoluminescence

Kelly S. Wilson[a], Madelyn N. Scott[a], Cathy Y. Wong[a,b,c,*]

[a] Department of Chemistry and Biochemistry, University of Oregon, Eugene, OR, 97403, USA
[b] Oregon Center for Optical, Molecular, and Quantum Science, University of Oregon, Eugene, OR, 97403, USA
[c] Materials Science Institute, University of Oregon, Eugene, OR, 97403, USA

ARTICLE INFO

Keywords:
Transient absorption spectroscopy
Excited state dynamics
Photoluminescence
Sulforhodamine
P3HT
In situ spectroscopy

ABSTRACT

Molecular aggregates and crystallites that emerge during the casting of semiconducting organic films from solution are highly sensitive to deposition conditions. Their structure determines the electronic properties, and ultimately the utility, of these materials as semiconductors. We report the development of a single-shot transient absorption (SSTA) spectrometer to measure the evolving excited state dynamics of organic molecules and polymers in situ during their casting into films from solution. The formation of molecular aggregates and crystallites changes the electronic structure, excited state dynamics, and concomitantly, the photoluminescence (PL) yield and structural heterogeneity. When these latter contributions are dynamic, they hinder accurate SSTA measurements of excited state dynamics. In this work, an additional optical chopper in the probe beam path is shown to correct for dynamic scatter and PL from the pump pulse. The importance of the correction provided by this optical chopping scheme to the measurement of photoluminescent and/or scattering samples is demonstrated using SSTA measurements of a sulforhodamine solution with high PL, a drop-cast sulforhodamine film with less PL, and a film of a prototypical organic semiconductor, poly(3-hexylthiophene-2,5-diyl).

1. Introduction

Many organic materials exhibit semiconducting behavior when electronically excited, and the utility of these materials as semiconductors depends on the dynamics of the excited state. For example, the efficiency of an organic photovoltaic depends on the rate of exciton migration and charge transfer [1], while the efficiency of an organic light emitting diode depends on the rate of electroluminescence relative to the rates of other competing processes [2]. The rates of these physical processes are commonly measured using time-resolved transient absorption (TA) spectroscopy [3–5]. In this spectroscopy, a pump pulse photogenerates excited species in the sample and a probe pulse is incident at the same location on the sample at a controlled time relative to the arrival time of the pump pulse. The time delay between the pump and probe pulses is typically controlled using a retroreflecting mirror on a motorized translation stage to vary the relative path lengths travelled by the two pulses. The probe pulse is directed to a detector to measure the transmission of the sample. An optical chopper is typically used to block alternate pump pulses, and successive transmission measurements by the probe are subtracted to obtain the differential transmission. This value can be normalized by total transmission and converted into differential absorption if desired.

While TA is a mature spectroscopy that has been successfully used to study a wide variety of biological and materials systems, this spectroscopy is generally restricted to the study of systems that are at structural equilibrium. The use of a retroreflector on a motorized delay stage requires that a separate measurement be performed at each pump-probe time delay in a transient, and the entire transient must usually be measured multiple times to attain a reasonable signal-to-noise ratio (SNR). This results in data acquisition times that range from a few minutes to multiple hours, depending on the optical density and response of the sample as well as the acceptable pulse energies of the pump and probe that avoid photodegradation. Owing to the data collection period needed when using TA in its conventional implementations, accurate measurement of the excited state dynamics is impossible for materials systems that are evolving on a timescale shorter than a few minutes, such as the formation of organic semiconducting films from solution. The measurement of these dynamic systems is of importance since solution processing is a scalable and economical manufacturing route for films [6], but can result in unpredictable device functionality [7] owing to the weak intermolecular interactions between organic molecules. Multiple kinetically trapped intermolecular geometries are

* Corresponding author at: Department of Chemistry and Biochemistry, University of Oregon, Eugene, OR, 97403, USA.
E-mail address: cwong3@uoregon.edu (C.Y. Wong).

https://doi.org/10.1016/j.synthmet.2019.03.007
Received 31 January 2019; Received in revised form 20 February 2019; Accepted 7 March 2019

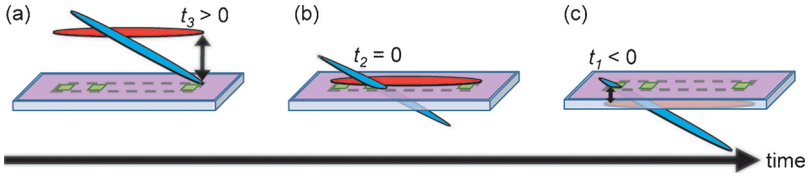

Fig. 1. Illustration of spatially encoded time delay. The pump pulse (blue) is tilted relative to the probe pulse (red), resulting in a linearly varying gradient of time delays between when the two pulses arrive at a sample (purple) on a glass substrate (grey). The relative angle between the pump and probe pulses determines the time delay at each spatial location, shown by the arrows in (a) and (c). The pump and probe both interact with the dashed rectangular region of the sample. Time zero occurs where the pump and probe pulses are spatially and temporally overlapped within the sample, shown in (b). In this example, time zero occurs at t_2, while t_1 and t_3 are before and after time zero, respectively (For interpretation of the references to colour in this figure legend, the reader is referred to the web version of this article).

possible, each with different electronic state structure, different excited state dynamics, and thus exhibit different physical properties [8,9]. The ability to measure excited state dynamics during the complex process of film formation will yield insight into how the functionality of a semiconducting organic film emerges from the photophysical properties of the solutions from which they are cast.

Multiple groups have attempted to bypass the limitations presented by TA in its typical implementations by spatially encoding the pump-probe time delays such that an entire transient can be collected in a single shot. There have been two general strategies for single-shot transient absorption (SSTA): the use of echelons and the use of tilted pulses. Echelon strategies involve enlarging the beam profile and transmitting [10,11] or reflecting [12,13] one of the pulses using an optic with a stair-like structure to impose different time delays on different spatial regions in the beam. For tilted pulse strategies, one beam is tilted with respect to the other beam to produce a gradient of pump-probe time delays at the sample [14–16], Fig. 1. The time delay range generated using this strategy is determined by the angle of the pump pulse relative to the sample plane (θ), the speed of light (c), and length (d) of the overlap region between the pump and probe on the sample.

$$t_{range} = d \sin(\theta) / c \quad (1)$$

In the past, the maximum pump-probe time delay acquired in a single-shot was limited to ~10 ps for tilted pulse techniques [15], and ~20 ps for echelon techniques [13]. In both transmissive and reflective echelons, scatter from the large number of edges present in an optic with this shape may limit the number of measurable time steps [17]. For transmissive echelon techniques, the accessible time range is limited by the thickness of the echelon optic. The regions of a pulse that traverse a thick section of the echelon are temporally delayed, but also experience a concomitant temporal elongation, reducing the time resolution of the measurement. When using the tilted pulse strategy the time resolution is not impacted in samples that are sufficiently thin, but the pump-probe time delay range can be limited by the Gaussian beam profile of the pulses used to spatially encode the time delay [16]. The excitation density will be higher in the center of the beam profile, which maps onto the center of the pump-probe time delay range. If the larger excitation density results in interactions between the excited species in one spatial region of the sample, the dynamics will be different in this part of the spatially encoded transient. The resulting transient will not accurately report the excited state dynamics of the system when in the linear regime. This can be avoided by lowering the power of the pump pulse, but this also lowers the SNR at the edges of the spatial profile, which map onto the beginning and end of the spatially encoded transient. In other words, the practically achievable time delay range is not merely determined by Eq. (1), but also by the SNR attained at each spatially encoded time delay when the entire measured region is excited in the linear regime. In our previous work [16], we overcame this obstacle by using a spatial light modulator (SLM) to flatten the spatial profile of the pump, enabling a larger part of the beam to be used. This resulted in a 45 ps spatially encoded pump-probe time delay range.

Normalized differential transmission is typically calculated by

$$\frac{\Delta T}{T} = \frac{T_{11} - T_{01}}{T_{01}} \quad (2)$$

where T_{11} is the measured intensity of the transmitted probe beam after the sample when the pump is also incident on the sample, and T_{01} is the intensity of the transmitted probe beam without the presence of the pump. The measurements of T_{11} and T_{01} are usually conducted sequentially using an optical chopper to block alternate pump pulses. Structural features in an organic film can cause some scatter from the pump pulse to reach the detector and contribute to the T_{11} term. Photoluminescence (PL) caused by the excitation of the pump pulse will also contribute to the T_{11} term. This is usually not a significant problem when measuring systems at structural equilibrium since the intensities of scatter and PL do not change during the measurement. Further, when using typical implementations of TA without spatial encoding, the measurement at each pump-probe time delay is conducted on a single spot on the sample that yields a certain amount of scatter and PL. Thus, in measurements of samples at structural equilibrium using typical implementations of TA, contributions to the signal from scatter of the pump beam or pump-induced PL constitute a constant baseline in the signal and can simply be subtracted. Pump scatter and pump-induced PL is a more significant problem when measuring organic films that are not at structural equilibrium since the amount of scatter and PL will change as the structure of the film evolves. Further, if the pump beam is incident on a larger region of the sample, as is the case in many implementations of SSTA, any heterogeneity in the film would result in a different amount of scatter at each location along the focal line. An evolving and heterogeneous sample in the spatial domain is a significant obstacle to the measurement of excited state dynamics during the process of film formation from solution.

In this work we report the use of an optical chopping scheme that enables the shot-to-shot correction of pump scatter and pump-induced PL. This scheme is conceptually similar to schemes reported in some two-dimensional electronic spectroscopy experiments [18,19] and proposed for other pump-probe measurements of chemical systems that are at structural equilibrium [20], but uses a 3:2 optical chopping ratio for the probe. We compare this with a more typical 2:2 probe chopping ratio. Our chopping scheme expands the ability of the SSTA technique to the measurement of changing excited state dynamics in organic small molecules and polymers as they form films from solution. This strategy is robust regardless of whether the amount of scatter or PL changes significantly during film formation. We demonstrate this capability by measuring a highly fluorescent solution of the organic small molecule dye sulforhodamine (SR), a film of SR, and a film of the prototypical organic semiconductor, poly(3-hexylthiophene-2,5-diyl) (P3HT) with and without shot-to-shot PL and scatter correction. The advance presented in this work will enable the measurement of excited state dynamics during the complex non-equilibrium processes that comprise solution-based organic film formation.

2. Experimental

Glass substrates (75 mm × 25 mm × 1 mm) were cleaned by sonication in methanol for 10 min. A film of sulforhodamine (SR) with an optical density of ~0.3 was produced by drop-casting a methanol solution onto a cleaned substrate at ambient conditions. A film of regioregular poly(3-hexylthiophene-2,5-diyl) (P3HT) was formed by spin-coating a chloroform solution onto a cleaned substrate in ambient

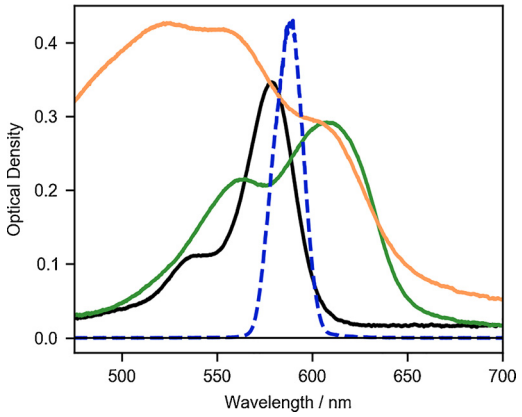

Fig. 2. Absorbance spectra. SR in solution (black), SR film (green), P3HT film (orange), and spectrum of laser pulse (blue dashed) (For interpretation of the references to colour in this figure legend, the reader is referred to the web version of this article).

conditions. A solution of SR in ethanol was measured in a cuvette with a 100 μm pathlength. Absorbance spectra are reported for each sample in Fig. 2, and images of the optical density of the films in their measured regions are included in Figure S1.

Transients were collected using a homebuilt SSTA instrument similar to previous descriptions [16,21] and described briefly here with changes emphasized. A 1 kHz Ti:sapphire laser (Coherent Astrella) and optical parametric amplifier produced pulses at 585 nm, Fig. 2. Optical Kerr effect measurements determined that the pulse duration at the sample was ~50 fs. As shown in Fig. 3a, a beam splitter divided each pulse into pump and probe pulses. The energies of the pump pulses were set using a waveplate and polarizer to 3.8 μJ for measurements of SR in solution and film and 1.0 μJ for measurements of P3HT film, with a pump:probe energy ratio of 11:1. Alternate pump pulses were blocked by an optical chopper. A second optical chopper was placed in the probe line, discussed below. The probe pulse was directed into a retroreflector mounted on a motorized translation stage. An iterative algorithm was used on half of the area of a phase-only spatial light modulator (SLM, Meadowlark) to produce a flat pump spatial profile by geometric beam shaping [16]. The other half of the SLM similarly flattened the spatial profile of the probe beam. After expanding both beams, they were focused to a 22.2 mm × 85 μm line on the sample plane using cylindrical lenses. The probe beam was incident normal to the sample, while the pump beam was tilted by $\theta = 54.2^{\circ}$ relative to the sample plane. The probe beam at the sample plane was imaged by a CMOS camera (Andor Zyla 5.5) with an exposure time of 0.9 ms. The probe illuminated 20 × 2560 pixels on the detector, and each of the 20 rows of pixels were summed together to provide a 1 × 2560 probe image. The film samples were repeatedly translated over a 15 mm region at a speed of 0.3 mm/s by a motorized linear actuator during the measurement, as shown in Fig. 3a. This averages over spatial heterogeneity in the films and makes the measurement robust to small fluctuations in optical density or film defects.

Two optical chopping schemes were compared. In optical chopping scheme A, Fig. 3b, the camera acquired images of the probe beam with the pump beam blocked (T_{01}) and unblocked (T_{11}) by using the optical chopper in the pump beam path. Further synchronization with the optical chopper in the probe beam path resulted in optical chopping scheme B which enabled the acquisition of images of pump scatter and pump-induced PL (T_{10}) and dark images with both pump and probe pulses blocked by the optical choppers (T_{00}). The optical chopper in the probe beam path had a duty cycle of 50%, with the phase set such that three pulses were transmitted followed by two pulses blocked, Fig. 3b. The process for calculating $\Delta T/T$ from each optical chopping scheme is detailed in Table 1 using the shot indices shown in Fig. 3b.

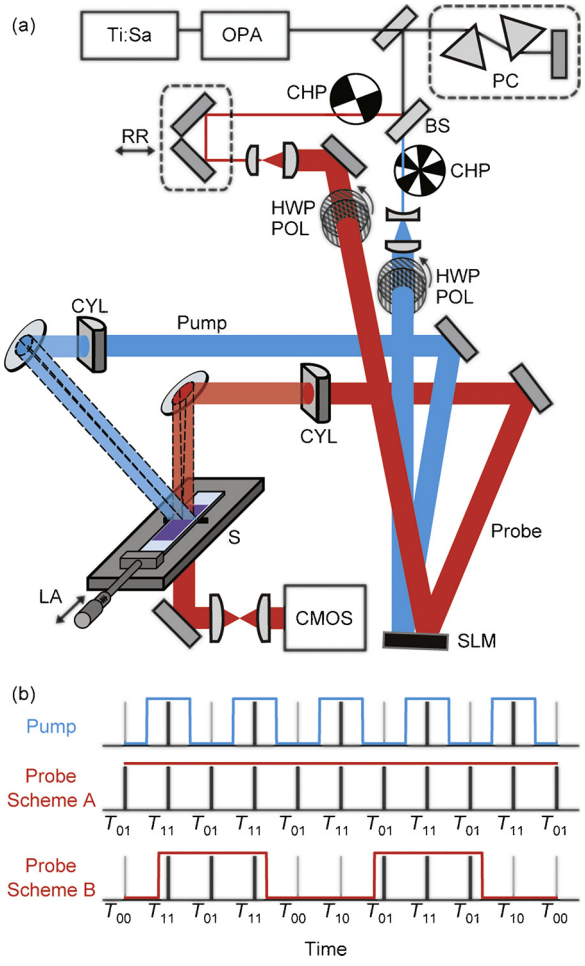

Fig. 3. Schematic of SSTA instrument and optical chopping schemes. (a) BS, beam splitter; CHP, optical chopper; CMOS camera; CYL, cylindrical lens; HWP, half-wave plate; LA, linear actuator; OPA, optical parametric amplifier; PC, prism compressor; POL, polarizer; RR, retroreflector; SLM, spatial light modulator; S, sample. (b) Optical chopping scheme used for the pump (blue) and schemes used for the probe (red) without (A) and with (B) the additional optical chopper in the probe beam path (For interpretation of the references to colour in this figure legend, the reader is referred to the web version of this article).

Table 1
Laser pulses used for successive measurements of $\Delta T/T$. Numbers correspond to the shot indices shown in Fig. 3b.

Data point	Scheme A	Scheme B
1	$\frac{2-1}{1}$	$\frac{(2-4)-(1-3)}{(1-3)}$
2	$\frac{4-3}{3}$	$\frac{(6-4)-(5-3)}{(5-3)}$
3	$\frac{6-5}{5}$	$\frac{(6-8)-(7-9)}{(7-9)}$
4	$\frac{8-7}{7}$	$\frac{(10-8)-(11-9)}{(11-9)}$

The spatially encoded time delay was calibrated by collecting the transients as a function of the position of the retroreflector in the probe line. “Time zero” occurred at the retroreflector location that resulted in spatial and temporal overlap of the pump and probe pulses within the sample. A sharp increase in the $\Delta T/T$ signal was observed at time zero owing to the creation of excited species. Time zero was unique for each pixel because of the tilt of the pump pulse, Fig. 4a. The line formed by the pixel location and retroreflector position at each time zero was used to determine that the time delay encoded by each pixel is 23.0 fs/pixel. The use of the SLM to flatten both the pump and the probe profiles

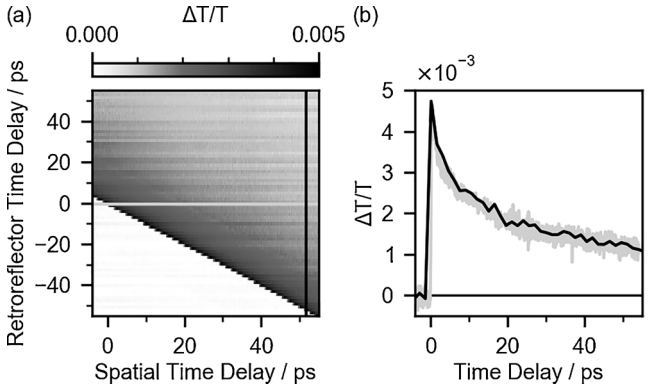

Fig. 4. Calibration of spatially encoded time delay. (a) SSTA measurements of a P3HT film at a range of retroreflector positions corresponding to steps of 1.5 ps. (b) Transients collected by SSTA in 5 s (grey) and by translation of retroreflector in 55 min (black).

enabled a 60 ps time delay range, an increase from 45 ps in our previous work where only the pump profile was flattened [16]. SSTA measurements were collected while holding the retroreflector at a static location. Horizontal cross sections of the plot in Fig. 4a represent transients measured by SSTA, while vertical slices of the plot are the equivalent of a typical TA measurement using a single pixel as a detector. The excited state dynamics measured using the spatially encoded SSTA time delay is shown to be identical to that measured by traditional TA in Fig. 4b. The incident pump power was lowered until the transients collected using pixels throughout the beam profile are found to be identical, confirming that the excitation density across the entire pump beam profile is either identical or below the threshold at which interactions between excited species play a role. This calibration and procedure is performed to confirm signal linearity for each measured sample.

3. Results and discussion

Normalized differential transmission is calculated by Eq. (2) in a typical TA measurement using optical chopping scheme A. Optical chopping scheme B of Fig. 3b enables the collection of two additional pulse combinations, T_{10} and T_{00}, when only the pump pulse is incident on the sample and when neither pulse is incident on the sample, respectively. The normalized differential transmission can then be calculated by Eq. (3).

$$\frac{\Delta T}{T} = \frac{(T_{11} - T_{10}) - (T_{01} - T_{00})}{T_{01} - T_{00}} \tag{3}$$

When measured and calculated in this way, $\Delta T/T$ represents the change in transmission owing to the presence of the pump pulse, excluding any contributions from pump scatter or pump-induced PL. Note that the intensity measured when neither beam is incident on the camera, T_{00}, is the result of stray light and dark current from the camera. The signal from T_{00} is present in each of the other pulse combinations, including T_{10}. Since T_{10} is being subtracted from the T_{11} term, T_{00} must also be subtracted from the T_{01} term. The T_{00} term is included in optical chopping scheme B to enable the dynamic subtraction of this contribution. However, if T_{00} is shown to not change with time, this measurement could potentially be acquired only once, either before or after the SSTA measurement. This would further reduce the time required to acquire enough signal to achieve an adequate SNR.

The use of a 3:2 optical chopping ratio for the probe pulses enables the acquisition of corrected transients using overlapping sets of four laser shots, as shown in Table 1. Two $\Delta T/T$ transients are calculated using laser shots 1 through 6, and another two $\Delta T/T$ transients are calculated using laser shots 6 through 11, where each transient is calculated using consecutive measurements of T_{11} or T_{01}. This 3:2 chopping ratio is advantageous over a 2:2 ratio because it increases the number of consecutive measurements of T_{11} and T_{01}. Using consecutive measurements optimizes the fidelity of the differential calculation since adjacent laser shots are more likely to have correlated energies [22]. The correlation in pulse energy and pointing may not be significantly stronger for consecutive shots than for temporally distant shots if laser noise sources are carefully controlled, but a measurement design that always collects T_{11} and T_{01} consecutively is preferred in the case of increased correlation between consecutive shots. The consecutive measurement of T_{11} and T_{01} is also important when the sample is spatially translated during the measurement to average over any spatial heterogeneity. In this work, the films are translated by 0.3 µm between successive shots, which is negligible in comparison to the 85 µm width of the focal line. In addition to optimizing the differential measurement by using sequential pulses, the 3:2 probe chopping ratio also increases the rate of SNR growth by using overlapping sets of four laser shots for each transient. Fig. 5 compares the growth of SNR during a measurement of SR solution when using the 3:2 ratio of chopping scheme B and a 2:2 chopping ratio, which does not use overlapping sets of laser shots to calculate $\Delta T/T$. Further details of this comparison are provided in Table S1.

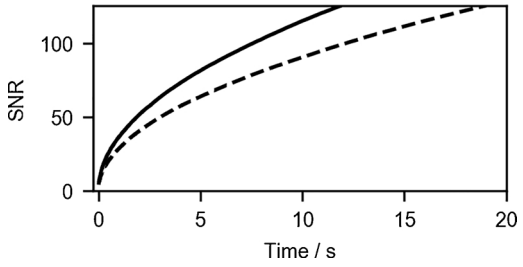

Fig. 5. Comparison of increasing SNR over time in the measured $\Delta T/T$ signal of SR in solution when using a 3:2 (solid) and 2:2 (dashed) optical chopping ratio for the probe.

Fig. 6a compares $\Delta T/T$ for a SR solution calculated using Eqs. (2) and (3), the equivalent of using optical chopping schemes A and B. The elevated baseline measured using optical chopping scheme A is comprised of pump scatter, pump-induced PL, stray ambient light, and dark current from the detector. This will be a constant baseline that can be simply subtracted if the sample is not changing and measured using a typical TA apparatus where the pump and probe beams are both focused to small spots on the sample. The baseline is automatically subtracted in optical chopping scheme B using Eq. (3). Fig. 6a shows the undesirable contribution from pump scatter and pump-induced PL, calculated by

$$\frac{T_{10} - T_{00}}{T_{01} - T_{00}}. \tag{4}$$

The contribution from stray ambient light and detector dark current are subtracted to isolate the contributions unique to the T_{10} measurement. The contribution of pump scatter and pump-induced PL to the baseline is not necessarily equal at all pixels when using a spatially encoded measurement technique, necessitating the measurement of the baseline at each pixel.

While the cuvette holding the SR solution may have scratches that cause spatially dependent scatter, the main source of the difference between the $\Delta T/T$ signal calculated using optical chopping schemes A and B is owing to the PL of the sample. The impact of the extra pump-induced signals on the measured $\Delta T/T$ signal depends on the PL yield of the sample, the number of scattering features at the sample, and the intensity of the change in sample transmission caused by photoexcitation by the pump, the latter of which is the desired signal. Fig. 6b shows the percentage of the acquired signal using optical chopping scheme A that is comprised of the undesired pump scatter and pump-induced PL, where we use the signal at 40 ps as the nominal amplitude of the

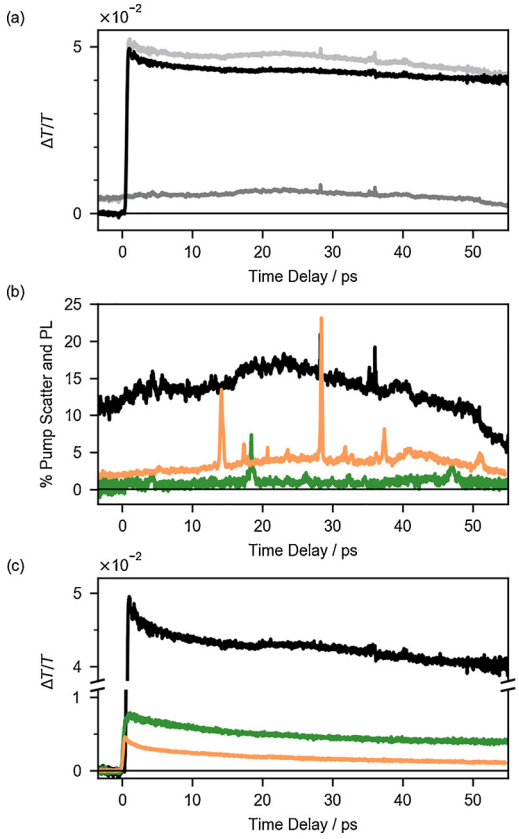

Fig. 6. Comparison of signal collected using optical chopping schemes A and B. (a) SSTA signal from SR solution collected using chopping scheme A (light grey), chopping scheme B (black), and the contribution of pump scatter and pump-induced PL as calculated using Eq.(4) (dark grey). (b) Percent of signal comprised by pump scatter and pump-induced PL for SR in solution (black), SR in a film (green), and P3HT (orange), calculated using the signal collected at a time delay of 40 ps using optical chopping scheme A as the nominal signal intensity. (c) Comparison of SSTA signal from SR solution (black), SR film (green), and P3HT (orange) using optical chopping scheme B after correction for pump scatter and PL using Eq. (3) (For interpretation of the references to colour in this figure legend, the reader is referred to the web version of this article).

acquired signal. While the SR solution is photoluminescent and thus the undesirable contributions calculated by Eq. (4) have greater intensity, the differential transmission caused by the excited states is also fairly strong ($\Delta T/T \sim 4 \times 10^{-2}$). Once the SR molecules aggregate and form a film they are not as photoluminescent, and while the film has more scattering features than the cuvette holding solution, the intensity of the undesirable contributions from scatter and PL is smaller in the film than in solution. Finally, the film of P3HT is neither highly fluorescent nor highly scattering, but the signal generated by P3HT at the pump intensities that prevent photodamage and interactions between excited species is also lower ($\sim 4 \times 10^{-3}$, Fig. 4c). The small amount of scatter and PL from the P3HT film still constitutes ~3% of the desired $\Delta T/T$ signal, with spikes of contribution from pump scatter at time delays corresponding to spatial locations on the film with structural features that cause a particularly large contribution from scatter.

It is noteworthy that the amount of pump scatter and pump-induced PL measured for SR is different for the solution and the film. It is common for the PL yield and PL spectrum of organic small molecules and polymers to change as they aggregate and crystallize owing to the formation of H- or J-aggregates that may exhibit weaker or stronger PL, respectively [23]. Without accounting for this changing PL, measurements of the excited state dynamics during molecular aggregation using SSTA would be incorrect owing to the evolving contribution of PL. Films are, generally, also highly scattering in comparison to solutions. Not accounting for this dynamic contribution could invalidate an SSTA measurement during film formation.

In summary, we have performed SSTA measurements on prototypical organic semiconducting films comprised of small molecules (SR) or conjugated polymers (P3HT) as well as small molecules in solution (SR) exhibiting high PL. An optical chopping scheme is presented that enables the shot-to-shot correction of pump scatter and pump-induced PL. This is the first demonstration of the use of a spatially encoded time delay to measure the excited state dynamics of organic films with shot-to-shot corrections for pump scatter and pump-induced PL. Since these two contributions are dynamic as molecules aggregate and structural features evolve, this advance enables SSTA to measure the excited state dynamics of organic molecules as they form solution-cast films.

Funding

This material is based upon work supported by the National Science Foundation under Grant No. 1752129.

Appendix A. Supplementary data

Supplementary material related to this article can be found, in the online version, at doi:https://doi.org/10.1016/j.synthmet.2019.03.007.

References

[1] G.J. Hedley, A. Ruseckas, I.D.W. Samuel, Light harvesting for organic photovoltaics, Chem. Rev. 117 (2017) 796–837, https://doi.org/10.1021/acs.chemrev.6b00215.
[2] A.S.D. Sandanayaka, T. Matsushima, C. Adachi, Degradation mechanisms of organic light-emitting diodes based on thermally activated delayed fluorescence molecules, J. Phys. Chem. C. 119 (2015) 23845–23851, https://doi.org/10.1021/acs.jpcc.5b07084.
[3] U. Megerle, I. Pugliesi, C. Schriever, C.F. Sailer, E. Riedle, Sub-50 fs broadband absorption spectroscopy with tunable excitation: putting the analysis of ultrafast molecular dynamics on solid ground, Appl. Phys. B 96 (2009) 215–231, https://doi.org/10.1007/s00340-009-3610-0.
[4] G. Lanzani, Pump Probe, Other modulation techniques, The Photophysics Behind Photovoltaics and Photonics, 1st edition, Wiley-VCH Verlag GmbH & Co. KGaA, 2012, p. 177.
[5] R. Berera, R. van Grondelle, J.T.M. Kennis, Ultrafast transient absorption spectroscopy: principles and application to photosynthetic systems, Photosynth. Res. 101 (2009) 105–118, https://doi.org/10.1007/s11120-009-9454-y.
[6] R.R. Sondergaard, M. Hosel, F.C. Krebs, Roll-to-Roll fabrication of large area functional organic materials, J. Polym. Sci. Pt. B-Polym. Phys. 51 (2013) 16–34, https://doi.org/10.1002/polb.23192.
[7] C.Y. Wong, B.D. Folie, B.L. Cotts, N.S. Ginsberg, Discerning variable extents of interdomain orientational and structural heterogeneity in solution-cast polycrystalline organic semiconducting thin films, J. Phys. Chem. Lett. 6 (2015) 3155–3162, https://doi.org/10.1021/acs.jpclett.5b01416.
[8] G. Giri, E. Verploegen, S.C.B. Mannsfeld, S. Atahan-Evrenk, D.H. Kim, S.Y. Lee, H.A. Becerril, A. Aspuru-Guzik, M.F. Toney, Z. Bao, Tuning charge transport in solution-sheared organic semiconductors using lattice strain, Nature 480 (2011) 504–508, https://doi.org/10.1038/nature10683.
[9] Y. Diao, L. Shaw, Z. Bao, S.C.B. Mannsfeld, Morphology control strategies for solution-processed organic semiconductor thin films, Energy Environ. Sci. 7 (2014) 2145–2159, https://doi.org/10.1039/c4ee00688g.
[10] G.P. Wakeham, K.A. Nelson, Dual-echelon single-shot femtosecond spectroscopy, Opt. Lett. 25 (2000) 505–507, https://doi.org/10.1364/OL.25.000505.
[11] P.R. Poulin, K.A. Nelson, Irreversible organic crystalline chemistry monitored in real time, Science 313 (2006) 1756–1760, https://doi.org/10.1126/science.1127826.
[12] H. Sakaibara, Y. Ikegaya, I. Katayama, J. Takeda, Single-shot time-frequency imaging spectroscopy using an echelon mirror, Opt. Lett., OL 37 (2012) 1118–1120, https://doi.org/10.1364/OL.37.001118.
[13] Y. Minami, H. Yamaki, I. Katayama, J. Takeda, Broadband pump–probe imaging spectroscopy applicable to ultrafast single-shot events, Appl. Phys. Exp. 7 (2014) 022402, https://doi.org/10.7567/APEX.7.022402.
[14] J.T. Fourkas, L. Dhar, K.A. Nelson, R. Trebino, Spatially encoded, single-shot ultrafast spectroscopies, J. Opt. Soc. Am. B 12 (1995) 155–165, https://doi.org/10.1364/JOSAB.12.000155.
[15] R. Weinkauf, L. Lehr, D. Georgiev, E.W. Schlag, Time multiplexing: a new single shot femtosecond pump-probe technique, Appl. Phys. B 64 (1997) 515–519, https://doi.org/10.1007/s003400050208.
[16] K.S. Wilson, C.Y. Wong, Single-shot transient absorption spectroscopy with a 45 ps pump-probe time delay range, Opt. Lett., OL 43 (2018) 371–374, https://doi.org/

10.1364/OL.43.000371.
[17] T. Shin, J.W. Wolfson, S.W. Teitelbaum, M. Kandyla, K.A. Nelson, Dual echelon femtosecond single-shot spectroscopy, Rev. Sci. Instrum. 85 (2014) 083115, https://doi.org/10.1063/1.4893641.
[18] R. Augulis, D. Zigmantas, Two-dimensional electronic spectroscopy with double modulation lock-in detection: enhancement of sensitivity and noise resistance, Opt. Exp., OE 19 (2011) 13126–13133, https://doi.org/10.1364/OE.19.013126.
[19] I.A. Heisler, R. Moca, F.V.A. Camargo, S.R. Meech, Two-dimensional electronic spectroscopy based on conventional optics and fast dual chopper data acquisition, Rev. Sci. Instrum. 85 (2014) 063103, https://doi.org/10.1063/1.4879822.
[20] C.A. Werley, S.M. Teo, K.A. Nelson, Pulsed laser noise analysis and pump-probe signal detection with a data acquisition card, Rev. Sci. Instrum. 82 (2011) 123108, https://doi.org/10.1063/1.3669783.
[21] K.S. Wilson, C.Y. Wong, In situ measurement of exciton dynamics during thin-film formation using single-shot transient absorption, J. Phys. Chem. A 122 (2018) 6438–6444, https://doi.org/10.1021/acs.jpca.8b06248.
[22] D. Polli, L. Lüer, G. Cerullo, High-time-resolution pump-probe system with broadband detection for the study of time-domain vibrational dynamics, Rev. Sci. Instrum. 78 (2007) 103108, https://doi.org/10.1063/1.2800778.
[23] F.C. Spano, C. Silva, H- and J-aggregate behavior in polymeric semiconductors, Annu. Rev. Phys. Chem. 65 (2014) 477–500, https://doi.org/10.1146/annurev-physchem-040513-103639.